

VIBRATION MEASUREMENTS OF THE GERBIL EARDRUM UNDER QUASI-STATIC PRESSURE STEPS

Orhun Kose¹, W. Robert J. Funnell^{1,2}, Sam J. Daniel^{3,2}

¹ Department of BioMedical Engineering, McGill University.

² Department of Otolaryngology – Head and Neck Surgery, McGill University

³ Department of Pediatric Surgery, McGill University

Contact info:

orhun.kose@mail.mcgill.ca

robert.funnell@mcgill.ca

sam.j.daniel@mail.mcgill.ca.

This version of the article was accepted for publication, after peer review, but is not the Version of Record and does not reflect post-acceptance improvements, or any corrections. The Version of Record is available online at <http://dx.doi.org/10.1007/s10162-020-00763-2> and at <https://rdcu.be/b6cOt> (View-only copy).

Use of this Accepted Version is subject to the publisher's Accepted Manuscript terms of use: <https://www.springernature.com/gp/open-research/policies/accepted-manuscript-terms>

ABSTRACT: Tympanometry is a relatively simple non-invasive test of the status of the middle ear. An important step toward understanding the mechanics of the middle ear during tympanometry is to make vibration measurements on the eardrum under tympanometric pressures. In this study, we measured in-vivo vibration responses in 11 gerbils while varying the middle-ear pressure quasi-statically, with the ear canal at ambient pressure. Vibrations were recorded using a single-point laser Doppler vibrometer with five glass-coated reflective beads (diameter $\sim 40 \mu\text{m}$) as targets. The locations were the umbo, mid-manubrium, posterior pars tensa, anterior pars tensa, and pars flaccida.

As described in earlier studies, the unpressurized vibration magnitude was flat at low frequencies, increased until a resonance frequency at around 1.8–2.5 kHz, and became complex at higher frequencies. At both the umbo and mid-manubrium points, when the static pressure was decreased to the most negative middle-ear pressure (-2500 Pa), the low-frequency vibration magnitude (measured at 1.0 kHz) showed a monotonic decrease, except for an unexpected dip at around -500 to -1000 Pa . This dip was not present for the pars-tensa and pars-flaccida points. The resonance frequency shifted to higher frequencies, to around 7–8 kHz at -2500 Pa . For positive middle-ear pressures, the low-frequency vibration magnitude decreased monotonically, with no dip, and the resonance frequency shifted to around 5–6 kHz at $+2500 \text{ Pa}$. There was more inter-specimen variability on the positive-pressure side than on the negative-pressure side. The low-frequency vibration magnitudes on the negative-pressure side were higher for the pars-tensa points than for the umbo and mid-manubrium points, while the magnitudes were similar at all four locations on the positive-pressure side. Most gerbils showed repeatability within less than 10 dB for consecutive cycles.

The results of this study provide insight into the mechanics of the gerbil middle ear under tympanometric pressures.

KEYWORDS: middle ear, eardrum, vibration, laser Doppler vibrometry, static pressure, tympanometry

INTRODUCTION

Tympanometry is a clinical test that gives information about the status of the middle ear, to detect conditions like the presence of middle-ear fluid, inflammation, infection and cholesteatoma (e.g., Kei et al. 2003). In tympanometry, a probe tip is placed in the ear canal to introduce a range of quasi-static pressures at the same time as a speaker generates an acoustical signal, which is recorded by a microphone. The speaker may introduce a pure-tone signal (e.g., 226 Hz is common for adult tympanometry), or a chirp (a short signal whose frequency changes with time). A tympanogram displays the measured acoustical input admittance as a function of the quasi-static pressure. The input admittance is sometimes hard to interpret in adults, and even more so for infants. Tympanometry is highly dependent on the behaviour of the eardrum, and studying the response of the eardrum with respect to simultaneous large quasi-static pressures and sound pressures can provide insight into the mechanics of the middle ear during tympanometry. Figure 1 shows a typical tympanogram; the input admittance measured at the entrance to the ear canal is displayed as a function of the static pressure for a single pressure sweep. The largest admittance occurs around 0 Pa.

As an intermediate step toward understanding the human middle ear, the use of animal models is widely accepted: they provide better-quality data and allow experiments that are not possible in humans. We use Mongolian gerbils for several reasons. There are abundant data available for both shape and vibration measurements of the gerbil eardrum and ossicles (e.g., Decraemer et al. 1997; Decraemer and Khanna 2000; Akache et al. 2007; Maftoon et al. 2013), which can be used to compare results and validate numerical models. The gerbil eardrum is large relative to the body size, which increases its accessibility. Gerbils have a hearing range that covers most of the human range and more, from about 200 Hz to 50 kHz (Engel 2008). Finally, when compared to chinchillas or larger animals, gerbils are inexpensive for both purchase and maintenance.

Several studies have involved LDV measurements at multiple points on the gerbil eardrum. For example, Ellaham (2007) measured post mortem at a few points on the pars tensa around the umbo, while de La Rochefoucauld & Olson (2010) performed both post-mortem and in-vivo vibration measurements at numerous points along the manubrium and on the pars tensa. More recently, Maftoon et al. (2013; 2014) measured in-vivo vibration responses along the manubrium and on the pars tensa in a line perpendicular to the manubrium close to its mid-point, as well as on the pars flaccida. Above a stiffness-dominated low-frequency region where all points were in phase, they observed a “breakup frequency” that ranged from 1.8 kHz to 2.8 kHz, beyond which many closely packed peaks were observed and the frequency response varied greatly among points, especially on the pars tensa.

In order to better understand the effects of tympanometry-like quasi-static pressures in the gerbil, several studies have introduced quasi-static pressures during measurements of eardrum shape (e.g., von Unge et al. 1993; Dirckx and Decraemer 2001; Gea et al. 2010) and admittance (von Unge et al. 1991), with the pressurization applied in the ear canal; and of umbo and pars-flaccida vibration (Lee and Rosowski 2001), with the pressurization in the middle ear. In a recent LDV study from our lab, Shapiro (2014) measured the vibrations at two locations on each of a small number of post-mortem gerbil eardrums with quasi-static pressures in the middle ear.

In this study we present in-vivo gerbil eardrum vibration measurements under static pressures using the step-wise pressure protocol used in (Dirckx and Decraemer 2001), but with the pressures applied in the middle-ear cavity as done by (Shapiro 2014). The measurements were made at two points on the manubrium, two on the pars tensa and one on the pars flaccida. The results are given for each point as frequency responses for different pressures and also as functions of pressure for a specific frequency. Differences between consecutive cycles and over the course of the experiment are shown.

MATERIALS & METHODS

Gerbil preparation

This study received ethics approval from the Institutional Review Board of the McGill University Health Centre Research Institute. The experiments were performed on male Mongolian gerbils (*Meriones unguiculatus*) provided by Charles River Laboratories (St-Constant, QC) with body weights ranging from 50 to 100 g. Of our 15 most recent gerbils, results are reported for the 11 which survived until the end of the experiment and for which there were no problems with pressurization. Carprofen and buprenorphine (20 and 0.05 mg/kg, respectively) were administered subcutaneously 30 minutes prior to the surgery. Pentobarbital and xylazine (35–50 and 10 mg/kg, respectively) were prepared according to the age of the animal (35 mg/kg if the animal was less than 6 months old and 50 mg/kg if 6 months old or older) and administered intraperitoneally.

The health and induction level of the gerbil were monitored using a portable monitoring device (PhysioSuite, Kent Scientific, Torrington, CT), measuring its heart rate and blood O₂ saturation level with a paw sensor. Induction level was also checked by the toe-pinch reflex approximately every 5 minutes. A maintenance dose of pentobarbital and xylazine (5–10 and 10 mg/kg, respectively) was given every 30 minutes or whenever needed; the xylazine dose was injected once after two pentobarbital doses. The animal was euthanized with a 3-times anaesthesia overdose when the measurements had been completed, or if the toe reflex was recovered and the anaesthetic level could not be restored.

An incision was made between the left shoulder and the jaw, followed by careful removal of the skin and soft tissue to expose the posterior inferior part of the bulla. The complete exposure of the region was performed methodically, in the order posteriorly, superiorly, anteriorly and finally inferiorly around the ear canal. Finally, the ear canal was removed down to the bony meatus, exposing the eardrum. Care was taken to avoid cutting nearby blood vessels and, in the case of superior facial artery branches where avoidance was not possible, they were cauterized immediately.

To expose the inferior region of the eardrum (providing a complete view of the manubrium and the cone of light), part of the bony meatus was drilled away. A 1-mm hole was also created on the superior-posterior surface of the bulla at least 20 mm away from the bony meatus to access the middle ear with the pressurization system. Care was taken to prevent any physical damage to the bulla and any debris on the eardrum.

Laser Doppler vibrometry

Immediately after exposing the eardrum and drilling the middle-ear pressurization hole, glass-coated plastic beads with an average diameter of 40 μm (A-RET, Polytec, Waldbronn, Germany) were carefully placed in five different regions of the eardrum using a micro brush (XS Artificer Layer, Games Workshop, Memphis, TN). These beads improve the reflection of the beam of the laser Doppler vibrometer (LDV). As seen in Figure 2, one bead (indicated by a blue filled circle in the figure) was placed at the umbo and another one (red) at the centre of the pars flaccida. Then, another bead (also blue in the figure) was placed between these, on the manubrium (referred to below as mid-manubrium). Two more beads (green) were placed on the pars tensa, anterior and posterior to the manubrium, at the level of the mid-manubrium bead. Shaded areas in the figure show the estimated range of placement of each bead across specimens. Due to the variability in gerbil anatomy and in the fixation of the acoustic coupler, there were variations in the angle of incidence of the laser beam. These variations are assumed to be negligible. All measurements within a given animal were recorded without repositioning of the coupler.

The overall experimental setup is shown in Figure 3. A 3D-printed acoustic coupler made of a polymer resin (VeroYellow, Stratasys, Valencia, CA) was fixed on the bony meatus using dental cement (Intermediate Restorative Material, Dentsply, York, PA; yellow area in figure). The same dental cement was also used to fix the pressurization tube to the hole in the bulla.

The acoustic coupler supported the microphone probe tube, the speaker tube and the ventilation tube. The speaker (ER-2, Etymotic Research, Elk Grove Village, IL) introduced sound into the ear canal via the acoustic coupler, and the resulting sound pressure level was recorded by the microphone (ER-7C, Etymotic Research). A 10-cm-long ventilation tube was used to prevent pressure and moisture build up in the ear canal. A single-point LDV (HLV-1000, Polytec, Waldbronn, Germany) was attached to the operating microscope (OPMI-1 H, Zeiss, Oberkochen, Germany), its laser targeting the beads on the eardrum through a 15-mm-diameter float-glass optical window (Edmund Optics Inc, Barrington, NJ), which had a BBAR anti-reflection coating for the specific wavelength of the laser and was placed at a 5° angle on the top of the coupler to further reduce reflections. The acoustical stimulus was a linear frequency sweep from 0.5 to 10 kHz in 128 ms with no pause between sweeps. The speaker voltage was kept constant. The sound pressure recorded by the microphone was at least 60 dB SPL at 0.5 kHz and stayed within 5 dB for the frequency range of 0.5 to 10 kHz. The reflected laser signal strength measured at the sensor head was at least 70% for all measurements.

The pressurization system consists of a peristaltic pump controlled by a microcontroller (Arduino Uno, SmartProjects, Strambino, Italy); a pressure sensor (20 INCH-D-4V, Allsensors, Morgan Hill, CA); and the tube that provides access to the middle ear. The speed of the pump motor was kept constant at its maximum. The resulting pressurization rate (4400 Pa/sec) was determined by the combined volume (about 0.2 mL) of the gerbil middle-ear cavity and the tubes and connections of the pressurization system. In contrast to clinical tympanometric practice, the static pressure was applied in the middle-ear cavity and not in the ear canal.

The LDV velocity measurements were recorded using the VibSoft software (Polytec). Ten consecutive chirps at a time were averaged in the time domain, then converted to the frequency domain using a Fast Fourier Transform. The normalized vibration velocity was then converted to displacement and both magnitude and phase were saved using a custom macro which automatically stored the data using a

standardized file-naming system and synchronized the timestamps between the vibration and pressure measurements. The pressurization system was controlled by a Python script that transferred pressure-step commands from the computer to the microcontroller. The pressurization protocol was similar to the one used by Dirckx and Decraemer (2001), with the static pressure varying over a range of ± 2500 Pa in 500-Pa increments. They actually applied their pressures in the ear canal, but reported them as equivalent middle-ear pressures. The pressure values here are reported in terms of the actual middle-ear pressure. The pressure was held for 10 seconds at each step, corresponding to about 7 or 8 chirp averages. Only chirp averages with a laser strength of more than 50% were considered (usually 4 or 5 chirp averages per step) to ensure a good signal-to-noise ratio. A full pressurization cycle consisted of decreasing from 0 Pa to -2500 Pa, increasing back to 0 Pa, increasing to $+2500$ Pa, and decreasing back to 0 Pa. The tolerance of the pressurization system was chosen to minimize the transient between pressure steps without introducing oscillations during the step. Hence, there was variability of up to ± 100 Pa in the static pressure at each pressure level. The pressure sensor was accurate to within 12 Pa.

Measurements

At the beginning of each experiment, at least three consecutive pressurization cycles at the bead on the umbo were recorded. After three or more cycles at each of one or more of the other beads had been recorded, one or more final cycles were recorded at the umbo before sacrifice. (Sometimes pressurization cycles were also measured after sacrifice, but they are not reported here.) The laser was manually aimed at the target bead at the beginning of each cycle, and re-aimed after each pressure step when needed. The time required for the manual re-aiming sometimes resulted in losing the measurement for the first one or more chirp averages for the new pressure value. Figure 4 shows an example of the middle-ear pressure (black line) and the resulting vibration magnitude measurements (red line) at a single frequency (1.0 kHz) as a function of time throughout one pressurization cycle. The pressure signal shows irregularities at the beginnings of some of the pressure steps (e.g., the upward spike in the -500 -to- -1000 -Pa transition at $t \approx 20$ s and the brief reversal in the -2500 -to- -2000 Pa

transition at $t \approx 60$ s) and in the middles of some pressure steps (e.g., the spike in the 0-Pa step at $t \approx 4$ s). These irregularities may be due to the control system for the pump; they are assumed to have negligible effects on the response of the middle ear because they are rather small and very brief. At each step, one chirp average is selected (green square markers). The selection was performed based on visual examination of complete frequency responses, not just a single frequency as shown in the figure, and using the following criteria in order of decreasing priority: having a stable frequency response that does not show noise artifacts; having one or more other chirp averages in the same pressure step with overall magnitude within 2 dB of the selected chirp; and not being in the first two seconds of the pressure step. Due to the difficulty of the manual tracking, some of the steps did not have a chirp average that met all of the criteria (e.g., at the -500 -Pa step at $t \approx 20$ s, all consecutive chirp averages differed by more than 2 dB). For such a step, the chirp average that satisfied the first criterion was selected, and confirmed by comparing the magnitude at the corresponding pressure steps of the other pressurization cycles for that bead. Especially near ambient pressure, the bead displacements were large in response to the quasi-static pressure change, which often caused the bead to move outside the ~ 35 - μm spot size of the laser beam.

Noise floor

All measurements were recorded in a sound-isolation chamber where the animal and the microscope were placed on an anti-vibration pad on a table. Nevertheless, building vibrations and the vibration of the motor of the pump were sometimes recorded by the LDV. Figure 5 shows the vibration levels measured at a point on the inside of the acoustic coupler for several animals, compared with the lowest vibration magnitude response measured in G31 (at mid-manubrium, -1500 Pa). The noise floor in the figure stays below 0.1 nm/Pa up to 10 kHz, apart from a noise peak at 0.55 kHz for one measurement. For the range of frequencies considered here, the measured magnitudes were at least an order of magnitude larger than the noise floor.

RESULTS

Interspecimen variability

Figure 6 shows the unpressurized vibration responses at the umbo for all 11 gerbils. The range of the closed-bulla in-vivo results in Figure 4 of Maftoon et al. (2013) is indicated by the shaded area. The low-frequency (from 0.5 to 1.8 kHz) magnitudes for our gerbils, with the exception of G35, were 27 to 66 nm/Pa at 1 kHz, lower than those of Maftoon et al. (63 to 115 nm/Pa). The low-frequency phases for our gerbils were -7° to -20° at 1 kHz, closer to zero than those of Maftoon et al. (-14° to -35°). The peak caused by the pars flaccida in some of the gerbils of Maftoon et al. was not present in any of our gerbils, possibly due to differences in the experimental setup and the presence of the pressurization system. The range of middle-ear resonance frequencies reported by Maftoon et al. was 1.5 to 2.0 kHz, narrower than our range of 1.3 to 2.6 kHz. (The peaks and troughs in the frequency responses represent maxima and minima of damped combinations of the natural modes of the spatially distributed system, as reflected at the particular location being measured. Such peaks are often loosely referred to as resonance peaks.) The phases at this resonance were close to -90° for all gerbils. For frequencies above 2.5 kHz, the vibration magnitudes and the frequencies of the peaks, as well as the phase values, vary more among ears than at lower frequencies. This variability is smaller than the differences caused by changing the static pressure to ± 500 Pa. In the following sections, individual responses are shown for animal G31 (shown with thick lines in Figure 6), since it was the only animal for which measurements were recorded for all four regions, and its responses were fairly representative.

Temporal variability

Here we present the temporal variability of the vibration magnitude and phase throughout the experiment for animal G31. Figure 7 shows the four consecutive cycles at the beginning of the experiment (solid lines), as well as four cycles roughly two hours later (dashed lines). After the very first pressurization cycle (solid black line), the low-frequency vibration magnitude (measured at 1 kHz) decreased by as much as 9 dB at the second cycle (solid red line), and then stayed within 3 dB for the

third (solid green line) and fourth (solid blue line) cycles. The decrease was smaller at frequencies higher than 4 kHz. Due to similar small changes after the first cycle for all ears, in Figure 6 the second pressurization cycle was displayed for each umbo measurement.

Just before sacrifice, after about 2 hours of measurements on other beads, the low-frequency vibration magnitude at the umbo had increased back to its original value for the first three cycles (black, red and green dashed lines, respectively). The low-frequency vibration magnitude decreased by 14 dB for the last cycle (blue dashed line). The variability for consecutive cycles is inconsistent, which may be partly due to the variability in the actual static pressures (± 100 Pa) of nominally unpressurized measurements. This variability was present in most ears, but was again smaller than the differences caused by changing the static pressure to ± 500 Pa.

Manubrium response

This section presents vibration responses at the two manubrium points (umbo and mid-manubrium) for gerbil G31. Figure 8 shows the negative-pressure (left panel) and positive-pressure (right panel) half-cycles of the second pressurization cycle at the umbo. For the first measurement at 0 Pa (solid black line in the left panel), the vibration magnitude increases as the frequency increases, from 49 nm/Pa at 0.5 kHz until a broad peak at 1.6 kHz (R1, filled circular marker), with a peak magnitude of 83 nm/Pa, and then decreases. In the roll-off region after the R1 peak, there is another peak (R2) almost buried at 3.2 kHz (filled square marker) with a peak magnitude of 17 nm/Pa. (The identification of R2 with this frequency is ambiguous when looking at this curve alone, but it seems to be consistent with what is seen after the unloading phase, as described below, and with observations both in consecutive cycles and in other ears.) Above about 3.6 kHz, the frequency response becomes complex. As the pressure is decreased from 0 Pa to -500 , -1000 , -1500 , -2000 and -2500 Pa (solid red, green, blue, orange, and cyan, respectively), the 0.5-kHz magnitude decreases rapidly until -1500 Pa, then more or less plateaus at about 1 nm/Pa. R1 and R2 both shift to higher frequencies, changing rapidly until -1500 Pa,

reaching 3.8 and 6.6 kHz with peak magnitudes of 0.32 and 8.4 nm/Pa, respectively. When the pressure is further decreased, R1 shifts back to lower frequencies and rises in magnitude, reaching 3.3 kHz with a peak magnitude of 1.6 nm/Pa at -2500 Pa; while R2 shifts to slightly higher frequencies and slightly larger magnitudes, reaching 8.0 kHz and 9.1 nm/Pa at -2500 Pa. The drops in the magnitudes of R1 and R2 to minima followed by rises were present in most gerbils, with the minimum occurring at -1000 or -1500 Pa. Several gerbils other than G31 also showed a minimum followed by a small rise in the lower-frequency magnitudes at these pressures.

As the pressure is increased through the same pressure levels back to 0 Pa in the unloading phase (dashed lines in left panel), the low-frequency magnitude increases back to about 34 nm/Pa (somewhat lower than the original value of 49 nm/Pa at the start of the pressurization cycle) and both R1 and R2 (empty circular and square markers, respectively) shift back to lower frequencies. By 0 Pa, R1 and R2 have shifted back to 1.8 kHz and 3.7 kHz, respectively, somewhat higher than their original values of 1.6 kHz and 3.2 kHz, with peak magnitudes similar to their original values. Depending on which cycle was considered, the peak frequency for R1 and R2 at the same pressure level varied by as much as ± 150 Hz. Hence, for more negative pressures where the peaks shifted less than 150 Hz, the peak frequency was considered to have stayed constant.

The positive-pressure half-cycle is shown in the right-hand panel of Figure 8. Overall, the positive-pressure half-cycle shows smaller changes in the vibration magnitude than the negative-pressure half-cycle does. The low-frequency magnitude decreases gradually as the pressure is increased, from 34 nm/Pa at 0 Pa to 5 nm/Pa at $+2500$ Pa. R1 (filled circular marker), at 1.7 kHz for 0 Pa, becomes very broad at 2.9 kHz for $+500$ Pa before disappearing for more positive pressures. In some other ears, R1 was visible at $+1000$ Pa as well. R2 (filled square marker) also shifts to higher frequencies but becomes sharper as the pressure becomes more positive, reaching a frequency of 9.6 kHz with a peak magnitude of 40 nm/Pa at $+2500$ Pa. As the pressure is decreased back to 0 Pa (dashed lines), the low-

frequency magnitude reaches about 60 nm/Pa (somewhat higher than its original value of 50 nm/Pa at the start of the negative-pressure half-cycle). R1 (empty circular marker) shifts back to 1.4 kHz, close to its original value of 1.6 kHz, while R2 (empty square marker) shifts back to 4.2 kHz, higher than its original value of 3.2 kHz. At each pressure level, the overall vibration magnitude is larger in the unloading phase than in the loading phase. This feature in the positive-pressure half-cycle was consistent across all gerbils, although the magnitude and frequency differences between loading and unloading were small in some gerbils.

Threshold criteria were used to identify the peaks. Most peaks exceeded a width threshold (200 Hz, measured at half height) and a height threshold (peak-to-base magnitude ratio greater than 1.05). If a peak was harder to identify, such as the nearly buried peaks at 0 Pa, it was confirmed in subsequent cycles at the same pressure level (or adjacent pressure levels where applicable) and for other gerbils (where the feature was in a similar frequency range). Any features that were not visible in other cycles were not considered as peaks. After a peak was identified, we confirmed that there was a corresponding positive slope in the phase.

Some of the trends seen in Figure 8 are illustrated in a different way in Figure 9, in which the frequencies and peak magnitudes of R1 (left panels) and R2 (right panels) are plotted as functions of the static pressure for all 11 gerbils. In the upper left panel, for G31, R1 is seen to quickly shift from 1.6 kHz at 0 Pa to 3.2 kHz at -1000 Pa, and then stay close to about 3 kHz for higher pressures. For other gerbils, the R1 frequency can shift to as high as 4.4 kHz (G21) or as low as 2.2 kHz (G22). In the positive-pressure half-cycle of G31, R1 shifts only slightly higher at +500 Pa and was not visible for more positive pressures. In other ears also, for positive pressures the R1 frequency usually shifted only slightly, with a few exceptions. In G28, R1 was still visible even at +1000 Pa. R2 (upper right panel) shifts to much higher frequencies than R1 does. For G31, R2 keeps shifting to higher frequencies until -2500 Pa, reaching around 8.0 kHz. In the positive-pressure half-cycle, R2 shifts to even higher

frequencies, reaching 9.6 kHz at +2500 Pa. The R2 frequencies are fairly similar from ear to ear in the negative-pressure half-cycle, varying from 6 to 9 kHz at -2500 Pa. In the positive-pressure half-cycle, the variability is much larger, with some ears showing a progressive shift to frequencies up to around 10 kHz, while others rise up to about 6 kHz. G22 is an exception, with the R2 frequency staying at about 3 kHz.

In the lower left panel of the figure, the R1 peak magnitude for G31 decreases as the static pressure decreases to -1500 Pa, and then increases slightly to 1.6 nm/Pa when the pressure is decreased further to -2500 Pa. The minimum occurs at -1000 Pa for some gerbils. The R1 peak magnitudes at -2500 Pa vary from 0.9 to 3.0 nm/Pa. The R1 peak magnitude decreases slightly in the positive-pressure half-cycle at pressures where it was visible. The R2 peak magnitude (lower right panel) for G31 stays almost constant throughout the cycle, but some gerbils show a slight decrease in the negative-pressure half-cycle, and a slight increase in the positive-pressure half-cycle. All of the gerbils tend to show larger magnitudes for positive pressures than for negative pressures.

Figure 10 shows the vibration responses for a point at the mid-manubrium, again for gerbil G31. The initial nominally unpressurized vibration in the left panel has a low-frequency magnitude of about 50 nm/Pa (the same magnitude as at the umbo). R1 has a broad peak at 1.6 kHz (the same frequency as at the umbo) with a magnitude of 77 nm/Pa (similar to the 83 nm/Pa seen at the umbo). R2 has a small peak at 3.6 kHz (close to the frequency of 3.2 kHz seen at the umbo) with a magnitude of 16 nm/Pa (similar to the 17 nm/Pa seen at the umbo). As the pressure is decreased, the low-frequency magnitude again decreases, this time to about 2 nm/Pa (compared to the 1 nm/Pa seen at the umbo). The R1 and R2 frequencies shift upward, reaching 2.7 kHz and 8.1 kHz, respectively, at -2500 Pa (compared with 3.3 and 8.0 kHz, respectively, at the umbo). A dip in magnitude, similar to what was observed at the umbo, occurs at about -1500 Pa, where the R1 peak magnitude drops to 0.3 nm/Pa. Similar to what was observed at the umbo, when the pressure is increased back to 0 Pa, the low-frequency magnitude

risers and the R1 and R2 peaks shift back to close to their original values. In the positive-pressure half-cycle, the low-frequency magnitude decreases from about 34 nm/Pa at 0 Pa to about 7.6 nm/Pa at +1500 Pa, then increases slightly to about 8.5 nm/Pa at +2500 Pa. The R1 broad peak at 2.0 kHz at 0 Pa shifts to about 2.8 kHz at +500 Pa and then becomes buried at about 3.0 kHz for more positive pressures, similar to what is seen at the umbo where the R1 peak becomes buried at about the same frequency and pressure. (Several gerbils showed a slight R1 peak up to +1000 Pa at the umbo and/or the mid-manubrium.) R2 shifts upward to 7.6 kHz at +1500 Pa before shifting back downward to 6.9 kHz at +2500 Pa. When the pressure is decreased back to 0 Pa, the low-frequency magnitude increases up to 52 nm/Pa, close to its original value of 50 nm/Pa. As seen at the umbo, the low-frequency vibration magnitudes (up to about 1.5 kHz) are higher in the unloading phase than in the loading phase. R1 and R2 shift back to 1.4 kHz and 3.2 kHz, respectively, compared with their original values of 1.6 kHz and 3.6 kHz. The low-frequency magnitude decreases more when the pressure is decreased to -2500 Pa than when it is increased to +2500 Pa, similar to what is seen at the umbo.

Pars-tensa response

Figure 11 shows the pressurized vibration responses for a point on the posterior pars tensa, again for G31. At the beginning of the negative-pressure half-cycle (solid black curve in left panel), the vibration magnitude increases with frequency from about 60 nm/Pa until a broad peak at 1.7 kHz (similar to the R1 peak at manubrial points) with a peak magnitude of 85 nm/Pa, immediately followed by a sharp minimum with a minimum magnitude of 60 nm/Pa at 2.3 kHz. There is then a double-peak feature with peak frequencies at 2.7 kHz (similar to the peak frequency of R2 on the manubrium) and 3.7 kHz, with individual peak magnitudes of 280 and 225 nm/Pa, respectively. When the pressure is decreased, the low-frequency (0.5-kHz) magnitude decreases to about 4 nm/Pa at -2500 Pa. At -500 Pa, the R1 peak is almost buried at about 2.8 kHz, and it is not seen at all at more negative pressures. The following minimum has already disappeared at -500 Pa. The R2 double-peak feature merges into a single peak, at higher frequencies, as the pressure is decreased, reaching as high as 8.1 kHz with a peak magnitude of

42 nm/Pa at -2500 Pa. When the pressure is increased back to 0 Pa, the low-frequency magnitude increases back to 71 nm/Pa; R1 shifts back to 1.7 kHz; the sharp minimum returns at 2.8 kHz; and R2 is visible as closely spaced peaks again, at 3.4 and 4.4 kHz. In the positive-pressure half-cycle, the low-frequency magnitude decreases gradually to 5.3 nm/Pa at $+1000$ Pa and stays approximately constant for more positive pressures. R1 and the following minimum shift to 2.9 kHz and 4.0 kHz at $+500$ Pa, and both disappear for pressures more positive than $+500$ Pa. R2 shifts to higher frequencies in a cluster of peaks, the earliest of them reaching 7.8 kHz at 55 nm/Pa by $+2500$ Pa. For some of the other pressurization cycles, the R2 peaks shift beyond 10 kHz. When the pressure is decreased back to 0 Pa, the low-frequency magnitude recovers back to 58 nm/Pa, similar to its original value of 61 nm/Pa; R1 reappears as a broad peak of 123 nm/Pa at 1.7 kHz, close to its original value; and R2 appears as a single peak at 2.5 kHz with a peak magnitude of 255 nm/Pa, close to the original double-peak values of 280 and 255 nm/Pa, respectively. For some of the other cycles measured in this gerbil, and for all three consecutive cycles in the other gerbil (G32) in which posterior pars-tensa responses were measured, R2 reappeared as a double-peak feature when the pressure was increased back to 0 Pa. (The anterior pars-tensa responses in G32 had similar vibration magnitudes for all pressure steps but R2 appeared as a single peak, even at 0 Pa.) Similar to what is seen at the manubrial points, the unloading curves for the positive-pressure half-cycle have higher magnitudes than the loading curves do at the same pressure levels, at least at frequencies lower than 5 kHz.

Figure 12 shows the peak frequencies and magnitudes for R1 and R2 on the posterior pars tensa over the pressure cycle, analogous to Figure 9. Posterior pars-tensa responses were recorded in 4 gerbils: G24, G30, G31, and G36. For G31, R1 (upper left panel) can only be identified for pressures between -1000 and $+1000$ Pa, and the pressure range was even smaller for other gerbils. The R1 frequency increases when pressure is applied. The R2 frequency (upper right panel) shows a monotonic increase as the pressure is decreased (with the exception of the value at -500 Pa for G36), reaching as high as

8.9 kHz at -2500 Pa, and there is little difference between the loading and unloading curves. In the positive-pressure half-cycle, except for G36, the R2 frequency increases rapidly until $+1000$ Pa, then stays approximately constant for more positive pressures, at frequencies similar to those of the negative-pressure half-cycle. For G36 the R2 frequency shifts much less. There is a large difference between the loading and unloading curves in the positive-pressure half-cycle for G31, especially for pressures more positive than $+1000$ Pa. When G36 is excluded, there is similar variability in the R2 frequencies in the negative-pressure and positive-pressure half-cycles. The R1 peak magnitudes (lower left panel) decreased (until the peak disappeared) when the pressure was either decreased or increased from 0 Pa. There was less variability among the gerbils in the negative-pressure half-cycle. The R2 peak magnitude (lower right panel) for G31 shows a sharp decrease from 0 Pa to -500 Pa, and then stays mostly constant for more negative pressures. The initial sharp decrease seen in G31 is smaller for some other gerbils. In the positive-pressure half-cycle, the R2 peak magnitude shows an irregular decrease, decreasing to a lower magnitude than in the negative-pressure half-cycle, except for G36, where the R2 peak magnitude increases slightly between 0 Pa and $+500$ Pa before decreasing monotonically. As the pressure is decreased back toward 0 Pa, the magnitude returns to nearly the value it had at the beginning of the negative-pressure half-cycle for all gerbils.

Pars-flaccida response

The pressurized vibration responses for a point on the pars flaccida of G31 are shown in Figure 13. At the beginning of the negative-pressure half-cycle (solid black curve in left panel), the vibration magnitude shows an almost buried peak at 1.4 kHz (R1 – circular marker, corresponding to the R1 observed on the pars tensa and manubrium), with a peak magnitude of 145 nm/Pa. After a broad peak at 2.2 kHz (R2 – square marker, corresponding to the R2 observed on the pars tensa and the manubrium) with a peak magnitude of 182 nm/Pa, and a small notch at 3.7 kHz, the vibration magnitude decreases steadily at about 35 dB/octave. This rate is calculated by fitting a line between the beginning of the descent, after the small peak around 3.7 kHz, and about 10 kHz. Unlike the manubrial and pars-tensa

points, an additional low-frequency peak (R0 – triangular marker) is visible at 0.75 Hz with a peak magnitude of 96 nm/Pa. This peak was only visible on the pars flaccida, and is designated R0 since it occurs at lower frequencies than R1. As the pressure becomes negative, however, the shape of the frequency response changes drastically. At –500 Pa, the 0.5-kHz magnitude is down to around 8 nm/Pa; the vibration magnitude increases slowly as the frequency increases until R0 at around 1.1 kHz; decreases rapidly until a sharp minimum at 2.0 kHz; then increases until a distinct R1 at 2.7 kHz; followed by numerous peaks and troughs at higher frequencies with R2 at 4.9 kHz. As the pressure is decreased further to –2500 Pa, the low-frequency magnitude decreases to about 2 nm/Pa; R0 becomes buried in the region before the sharp minimum at around 1.8 kHz; and R1 and R2 shift to higher frequencies, reaching 3.7 and 8.1 kHz, respectively, by –2500 Pa. When the pressure has returned back to 0 Pa, R0 is barely visible at 0.8 kHz with a peak magnitude of 25 nm/Pa; the sharp minimum before R1 disappears; and R1 and R2 shift back to around 1.5 kHz and 4.1 kHz, with peak magnitudes of 38 and 14 nm/Pa, respectively. Numerous peaks and troughs at frequencies higher than R1 are still visible, unlike the original smooth frequency-response shape at the beginning of the cycle.

In the positive-pressure half-cycle (right-hand panel), as the pressure is increased from 0 Pa to +500 Pa, the peak magnitudes of R0, R1, and R2 actually increase slightly. (This increase in magnitudes was larger for other pressurization cycles, where they increased significantly between 0 Pa and +500 Pa or +1000 Pa.) As the pressure is then made more positive, R0 disappears, and R1 and R2 shift to higher frequencies; their peak magnitudes start to decrease after +1000 Pa for R1 and after +1500 Pa for R2. R1 and R2 reach 3.3 and 6.7 kHz, respectively, at +2500 Pa. When the pressure is decreased back to nominally 0 Pa, the frequency response (dashed black curve in right panel) returns nearly to the shape of the original curve (solid black curve in left panel), with the 500-Hz magnitude now at 100 nm/Pa (larger than its original value of 58 nm/Pa); followed by R0 and an almost buried R1 at 0.64 and 1.3 kHz (somewhat lower than their original values of 0.75 and 1.4 kHz), followed by a broad R2 at

1.9 kHz (somewhat lower than its original value of 2.3 kHz) with a peak magnitude of 163 nm/Pa (somewhat lower than its original 182 nm/Pa); followed by a steady decrease of about 35 dB/octave (the same as originally).

The behaviour of the frequencies and magnitudes of R1 and R2 as functions of the static pressure are shown for the pars flaccida in Figure 14. Pars-flaccida responses were recorded in G31 and G32. In the negative-pressure half-cycle, the R1 frequencies (upper left panel) for both G31 and G32 shift gradually from around 1.4 kHz at 0 Pa to higher frequencies for both negative and positive pressures. The R1 frequency for G31 is higher than that of G32 at all pressure levels, reaching 3.7 and 3.3 kHz at -2500 and $+2500$ Pa, respectively. The R2 peak frequency of G31 (upper right panel) starts at 1.9 kHz at 0 Pa, and shifts more than R1 does, reaching 8.1 and 6.8 kHz at -2500 and $+2500$ Pa, respectively. The R2 frequencies of G32 are mostly lower than those of G31, with a few exceptions between 0 Pa and $+1000$ Pa where they are similar. The R2 frequency of G31 shifts less in the positive-pressure half-cycle than in the negative-pressure half-cycle (the opposite of what happens on the manubrium), but this is not the case for G32.

The R1 and R2 peak magnitudes (lower left panel) for G31 both decrease when the pressure becomes less than zero. As the pressure is increased back to zero, the R1 peak magnitude increases to much higher than its original value. In the positive-pressure half-cycle, the R1 peak magnitude decreases as the pressure becomes positive. When the pressure is decreased back to zero, the R1 peak magnitude increases only until $+500$ Pa, and returns to its original value. G32 shows similar behaviour except that the magnitude changes are smaller, and the largest peak magnitudes occur at $+500$ Pa and $+1000$ Pa in the loading and unloading phases, respectively. The R2 peak magnitude (lower right panel) for G31 shows a distinct dip at -1000 Pa, whereas for G32 the R2 peak magnitude shows smaller and less regular changes, and the largest peak magnitudes occur at -500 Pa and $+500$ Pa in the unloading phases for the negative-pressure and positive-pressure half-cycles, respectively. The dip in the R2 peak

magnitude seen here for G31 was not observed in all pressurization cycles for that ear, nor for G32, and was thus not as consistent as the similar dip of the manubrium response. The R1 and R2 peak magnitudes (for both G31 and G32) start at similar values at 0 Pa, but the R1 peak magnitude decreases to a fraction of the R2 peak magnitude at -2500 Pa (a quarter for G31 and less than half for G32). Even though the R1 and R2 peak magnitudes varied between G31 and G32, the low-frequency magnitude behaviours were similar in all cycles.

DISCUSSION

In this study, we performed in-vivo vibration measurements on 11 gerbil ears under quasi-static pressure steps in the middle-ear cavity while the ear canal was kept at ambient pressure with a ventilation tube. The vibration responses at the umbo when both sides of the eardrum were at ambient pressure were fairly consistent with previous studies (Maftoon et al. 2013). Our frequency responses had an overall larger range across ears with generally lower magnitudes and higher frequencies of the peaks. These differences could be due to dehydration during preparation, when both the eardrum and the middle-ear were exposed. Rehydration between cycles was not possible due to the fixation of the acoustic coupler to the bony ear canal and the fixation of the pressurization tube in the bulla. The effects of dehydration have been studied during various middle-ear vibration measurements (e.g., Gyo et al. 1986; Rosowski et al. 1990; Voss et al. 2001; Kei et al. 2003; Ellaham et al. 2007; Maftoon et al. 2013). Maftoon et al. (2013) measured a maximum peak shift to higher frequencies of about 2 Hz/min, and a maximum peak magnitude decrease of about 0.2 %/min, over a time span of 90 minutes for the unpressurized vibration response at the umbo. This shift was within the variability in our results over the time span of two hours, but our measurements did not show a consistent shift.

The overall vibration magnitude decreased significantly after the first ever pressurization cycle, possibly due to preconditioning. Another factor that may have contributed to this change is the variability in the static pressure (up to ± 100 Pa) at each step. However, these cycle-to-cycle changes in

vibration magnitudes at any given pressure, even over a period of two hours, were smaller than the changes caused by the presence of static pressure.

When a static pressure was applied, the low-frequency magnitude decreased, and the peak frequencies shifted to higher frequencies. These changes were more rapid at pressures closer to zero, and started to plateau for pressures closer to ± 2500 Pa. The changes were greater, in both magnitudes and frequencies, for negative ear-canal pressures than for positive ones for all points on the eardrum, except for some cycles on the pars flaccida in some ears. These trends are consistent with previous gerbil vibration measurements, both unpressurized (Rosowski et al. 1999; de La Rochefoucauld and Olson 2010) and pressurized (Lee and Rosowski 2001; Shapiro 2014), and also with pressurized gerbil eardrum shape measurements (von Unge et al. 1993; Dirckx and Decraemer 2001; Gea et al. 2010). For both manubrial points, the low-frequency magnitude and the R1 peak magnitude each showed a dip at -1000 to -1500 Pa, depending on the cycle. Even though the magnitude difference was small in some ears, the presence of the dip was fairly robust. This phenomenon may be due to a buckling of the eardrum, or perhaps to some effect in the ossicular chain. Lee and Rosowski (2001) observed a similar dip in magnitude at the umbo (but not on the pars flaccida) around -2000 Pa, for frequencies between 1 and 6 kHz.

There were generally also magnitude differences, sometimes small, between the loading and unloading curves for both negative and positive pressurization half-cycles. For the negative-pressure half-cycle, the vibration magnitudes were higher in the loading phase than in the unloading phase, and vice-versa for the positive-pressure half-cycle (except for some positive-pressure steps on the pars flaccida). This was seen to some extent in all ears. This difference could be due to hysteresis. Hysteresis in response to quasi-static pressures on the gerbil eardrum has been reported before. For example, pressurized moiré measurements of eardrum shape resulted in hysteresis loops (e.g., von Unge et al. 1993; Dirckx and

Decraemer 2001), and Lee and Rosowski (2001) observed differences in the peak magnitude and frequency of vibrations for different directions of the pressure steps.

The overall vibration magnitudes at the mid-manubrium and at the umbo were similar at any given pressure, slightly larger at the mid-manubrium in some ears. (Maftoon et al. 2013) observed a systematic difference with the unpressurized umbo vibration magnitude being larger than that at the mid-manubrium, consistent with the classical view of rotation of the malleus around a fixed axis of rotation. The lack of a clear difference in magnitude here may be attributable, at least in part, to the inaccuracy (± 100 Pa) of our pressure steps.

Both manubrial points showed another peak at higher frequencies (R2 in the Results section), which became more distinct and shifted to higher frequencies when the pressure became either more negative or more positive. The amount that the R2 frequency shifted changed from location to location. For the posterior pars tensa, R2 showed as a double peak; Maftoon et al. (2013) also observed a double-peak feature at a similar location on the eardrum. In the positive-pressure half-cycle, R2 appeared as a series of closely-spaced peaks. The anterior pars-tensa frequency response was similar in shape to those of the manubrial points, but with larger overall magnitudes at the same pressure levels. The double-peak feature in the negative-pressure half-cycle on the posterior pars tensa, and the closely spaced peaks in the positive-pressure half-cycle, suggest that R2 may be a superimposition of small peaks on the manubrium but that these peaks become separate at some pressures on the pars tensa. The R1 and R2 peak heights both became larger at non-zero pressures, but the peak widths stayed mostly constant as pressure was decreased beyond -500 Pa or increased beyond $+500$ Pa. In some measurements, especially on the pars flaccida, the R1 and R2 peaks were close in frequency at 0 Pa, but ended up much further apart when the pressure was decreased. They reacted differently to the static pressure, presumably because different parts of the middle ear contributed differently when the pressure was decreased.

The pars-flaccida unpressurized frequency response was similar in shape to the manubrial response as well, with a few exceptions. The magnitude was significantly larger, as observed previously (Merchant et al. 1997; Rosowski et al. 1999; Lee and Rosowski 2001; Maftoon et al. 2013); a pars-flaccida peak (R0 in the Results section) appeared at 0.7 kHz, which was also previously reported (Lee and Rosowski 2001; Maftoon et al. 2013). R1 and R2 were present as almost buried peaks, similar to what was seen for the manubrial points. As the pressure was decreased to -500 Pa and below, however, the R0, R1, and R2 peaks became distinct with local minima between the peaks. This change in mode is consistent with the large deformation of the pars flaccida in the presence of even small static pressures. Dirckx et al. (1998) observed such large deformations for pressures as small as ± 100 Pa. Teoh et al. (1997) suggested that the pars flaccida's larger deformation could be limiting the deformation of the pars tensa, effectively stiffening the pars tensa and ossicular chain.

In this study, we aimed to provide insight into the effects of middle-ear-cavity static pressures on the vibration response of the gerbil eardrum. We developed an in-vivo gerbil ear model and observed the vibration responses at multiple locations. The vibration responses over a wide frequency range for multiple pressurization cycles were given and the main resonance peaks were identified. These pressure-step responses will be useful for validating numerical models of the gerbil middle ear in conjunction with previous shape and vibration measurements that involved pressure steps. For more direct relevance to tympanometry, it will be necessary to apply the quasi-static pressures in the ear canal rather than in the middle ear, and to perform similar multiple-point vibration measurements with a sweep pressure input, which is more difficult experimentally because of the need to track the beads throughout the pressurization sweep. In the meantime, these data do provide some insight into the effects of normal and pathological changes in middle-ear pressure as reflected in clinically observed variations of the tympanometric peak pressure (TPP) due to Eustachian tube function (e.g., the interval between swallows) and dysfunction (blockage).

Acknowledgements

The authors would like to thank Dr. Aurore Dodelet-Devillers for her help with the handling of the animals, anesthesia, and surgical procedures; Dr. Ross Wagner for his help in the development of the acoustic coupler and the experimental setup; Mr. Sajjad Feizollah and Dr. Majid Soleimani for their help with the surgical procedure; and the McGill University Health Centre Research Institute Vivarium staff for their help in maintaining and advising on the health and comfort of the animals. This work was supported in part by the Canadian Institutes of Health Research, the Natural Sciences and Engineering Research Council (Canada), the Fonds de recherche en santé du Québec, the Montréal Children's Hospital Research Institute, and the McGill University Health Centre Research Institute.

Conflict-of-interest disclosure statement

The authors declare that they have no conflict of interest.

References

- Akache F, Funnell WRJ, Daniel SJ (2007) An experimental study of tympanic membrane and manubrium vibrations in rats. *Audiol Neurootol* 12:49–58. <https://doi.org/10.1159/000097247>
- de La Rochefoucauld O, Olson ES (2010) A sum of simple and complex motions on the eardrum and manubrium in gerbil. *Hear Res* 263:9–15
- Decraemer WF, Khanna SM (2000) Three-dimensional vibration of the ossicular chain in the cat. pp 401–411
- Decraemer WF, Khanna SM, Funnell WRJ (1997) Vibrations of the cat tympanic membrane measured with high spatial resolution. St. Petersburg Beach, FL.
- Dirckx JJJ, Decraemer WF (2001) Effect of middle ear components on eardrum quasi-static deformation. *Hear Res* 157:124–137. [https://doi.org/10.1016/S0378-5955\(01\)00290-8](https://doi.org/10.1016/S0378-5955(01)00290-8)
- Dirckx JJJ, Decraemer WF, von Unge M, Larsson C (1998) Volume displacement of the gerbil eardrum pars flaccida as a function of middle ear pressure. *Hear Res* 118:35–46. [https://doi.org/10.1016/S0378-5955\(98\)00025-2](https://doi.org/10.1016/S0378-5955(98)00025-2)
- Ellaham NN, Akache F, Funnell WRJ, Daniel SJ (2007) Spatial vibration patterns of the gerbil eardrum. *Can Acoust* 35:38–39
- Engel J (2008) Gerbils can tune in. *J Physiol* 586:919. <https://doi.org/10.1113/jphysiol.2007.150409>
- Gea SLR, Decraemer WF, Funnell WRJ, et al (2010) Tympanic membrane boundary deformations derived from static displacements observed with computerized tomography in human and gerbil. *J Assoc Res Otolaryngol* 11:1–17. <https://doi.org/10.1007/s10162-009-0192-9>
- Gyo K, Goode RL, Miller C (1986) Effect of middle ear modification on umbo vibration: human temporal bone experiments with a new vibration measuring system. *Arch Otolaryngol Neck Surg* 112:1262–1268
- Kei J, Allison-Levick J, Dockray J, et al (2003) High-frequency (1000 Hz) tympanometry in normal neonates. *J Am Acad Audiol* 14:20–8. <https://doi.org/10.3766/jaaa.14.1.4>
- Lee C-Y, Rosowski JJ (2001) Effects of middle-ear static pressure on pars tensa and pars flaccida of gerbil ears. *Hear Res* 153:146–163. [https://doi.org/10.1016/S0378-5955\(00\)00269-0](https://doi.org/10.1016/S0378-5955(00)00269-0)
- Maftoon N, Funnell WRJ, Daniel SJ, Decraemer WF (2013) Experimental study of vibrations of gerbil tympanic membrane with closed middle ear cavity. *J Assoc Res Otolaryngol* 14:467–481. <https://doi.org/10.1007/s10162-013-0389-9>
- Maftoon N, Funnell WRJ, Daniel SJ, Decraemer WF (2014) Effect of opening middle-ear cavity on vibrations of gerbil tympanic membrane. *J Assoc Res Otolaryngol* 15:319–334. <https://doi.org/10.1007/s10162-014-0442-3>
- Merchant SN, Ravicz ME, Puria S, et al (1997) Analysis of middle ear mechanics and application to diseased and reconstructed ears. *Otol Neurotol* 18:139–154

- Rosowski JJ, Davis PJ, Donahue KM, et al (1990) Cadaver middle ears as models for living ears: comparisons of middle ear input immittance. *Ann Otol Rhinol Laryngol* 99:403–412. <https://doi.org/10.1177/000348949009900515>
- Rosowski JJ, Ravicz ME, Teoh SW, Flandermeyer D (1999) Measurements of middle-ear function in the Mongolian gerbil, a specialized mammalian ear. *Audiol Neurotol* 4:129–136
- Shapiro R (2014) An experimental study of vibrations in the gerbil middle ear under static pressure
- Teoh SW, Flandermeyer DT, Rosowski JJ (1997) Effects of pars flaccida on sound conduction in ears of Mongolian gerbil: acoustic and anatomical measurements. *Hear Res* 106:39–65. [https://doi.org/10.1016/S0378-5955\(97\)00002-6](https://doi.org/10.1016/S0378-5955(97)00002-6)
- von Unge M, Decraemer WF, Bagger-Sjöbäck D, Dirckx JJ (1993) Displacement of the gerbil tympanic membrane under static pressure variations measured with a real-time differential moire interferometer. *Hear Res* 70:229–242. [https://doi.org/10.1016/0378-5955\(93\)90161-S](https://doi.org/10.1016/0378-5955(93)90161-S)
- Voss SE, Rosowski JJ, Merchant SN, Peake WT (2001) Middle-ear function with tympanic-membrane perforations. I. Measurements and mechanisms. *J Acoust Soc Am* 110:1432–1444

Captions

Figure 1: A typical tympanogram of a newborn at 1 kHz.

Figure 2: Diagram (left) and photograph (right) of bead placement (blue=manubrium, green=pars tensa, red=pars flaccida; shaded areas represent ranges of bead placement; grey areas represent overhang of the bulla).

Figure 3: Experimental setup, with a plastic coupler fixed to the gerbil bony meatus. The static pressure was applied to the middle-ear cavity.

Figure 4: Middle-ear pressure (black) and corresponding vibration response (red) at 1.0 kHz for gerbil G31 at the umbo, for a single cycle. Green squares mark the measurements that were manually selected for each pressure step.

Figure 5: Noise floors of the vibration response (thin grey lines) for several gerbils as measured on the inside of the acoustic coupler. The vibration response with the lowest overall magnitude (G31, mid-manubrium, at -1500 Pa) is provided for comparison (thick black line).

Figure 6: Unpressurized vibration magnitudes (top) and phases (bottom) at the umbo for all 11 gerbils. Grey areas are the vibration magnitude and phase ranges for the 12 gerbils reported in Maftoon et al. (2013).

Figure 7: Nominally unpressurized in-vivo vibration magnitudes (top) and phases (bottom) at the umbo for four consecutive cycles at the beginning of the experiment (solid lines) and near the end of the experiment (dashed lines), for gerbil G31. The time of each measurement (in minutes after the first measurement) is given in the legend. (Actual middle-ear pressure values are given in parentheses.)

Figure 8: Vibration response of G31 at the umbo for negative-pressure half-cycle (left) and positive-pressure half-cycle (right). Solid curves = loading phase, dashed = unloading phase. Circles (R1) and squares (R2) show the locations of the resonances in the loading (filled symbols) and unloading (empty symbols) phases. (Actual middle-ear pressure values are given in parentheses for both loading and unloading phases.)

Figure 9: Behaviour of frequency-response peaks (as defined in the text) at the umbo, as functions of middle-ear pressure, for all 11 gerbils. Left panels = R1, right panels = R2. Top panels = peak frequency, bottom panels = peak magnitude. The green arrow indicates the dip in magnitude mentioned in the text.

Figure 10: Vibration response of G31 at the mid-manubrium for negative-pressure half-cycle (left) and positive-pressure half-cycle (right). Solid curves = loading phase, dashed = unloading phase. Circles (R1) and squares (R2) show the locations of the resonances in the loading (filled symbols) and unloading (empty symbols) phases. (Actual middle-ear pressure values are given in parentheses for both loading and unloading phases.)

Figure 11: Vibration response of G31 at the posterior pars tensa for negative-pressure half-cycle (left) and positive-pressure half-cycle (right). Solid curves = loading phase, dashed = unloading phase. Circles (R1) and squares (R2) show the locations of the resonances in the loading (filled symbols)

and unloading (empty symbols) phases. (Actual middle-ear pressure values are given in parentheses for both loading and unloading phases.)

Figure 12: Behaviour of frequency-response peaks (as defined in the text) at the posterior pars tensa, as functions of the middle-ear pressure, for four gerbils. Left panels = R1, right panels =R2. Top panels = peak frequency, bottom panels = peak magnitude.

Figure 13: Vibration response of G31 at the pars-flaccida for negative-pressure half-cycle (left) and positive-pressure half-cycle (right). Solid curves = loading phase, dashed = unloading phase. Circles (R1) and squares (R2) show the locations of the resonances in the loading (filled symbols) and unloading (empty symbols) phases. (Actual middle-ear pressure values are given in parentheses for both loading and unloading phases.)

Figure 14: Behaviour of frequency-response peaks (as defined in the text) at the pars flaccida, as functions of the middle-ear pressure, for gerbils G31 and G32. Left panels = R1, right panels =R2. Top panels = peak frequency, bottom panels = peak magnitude.

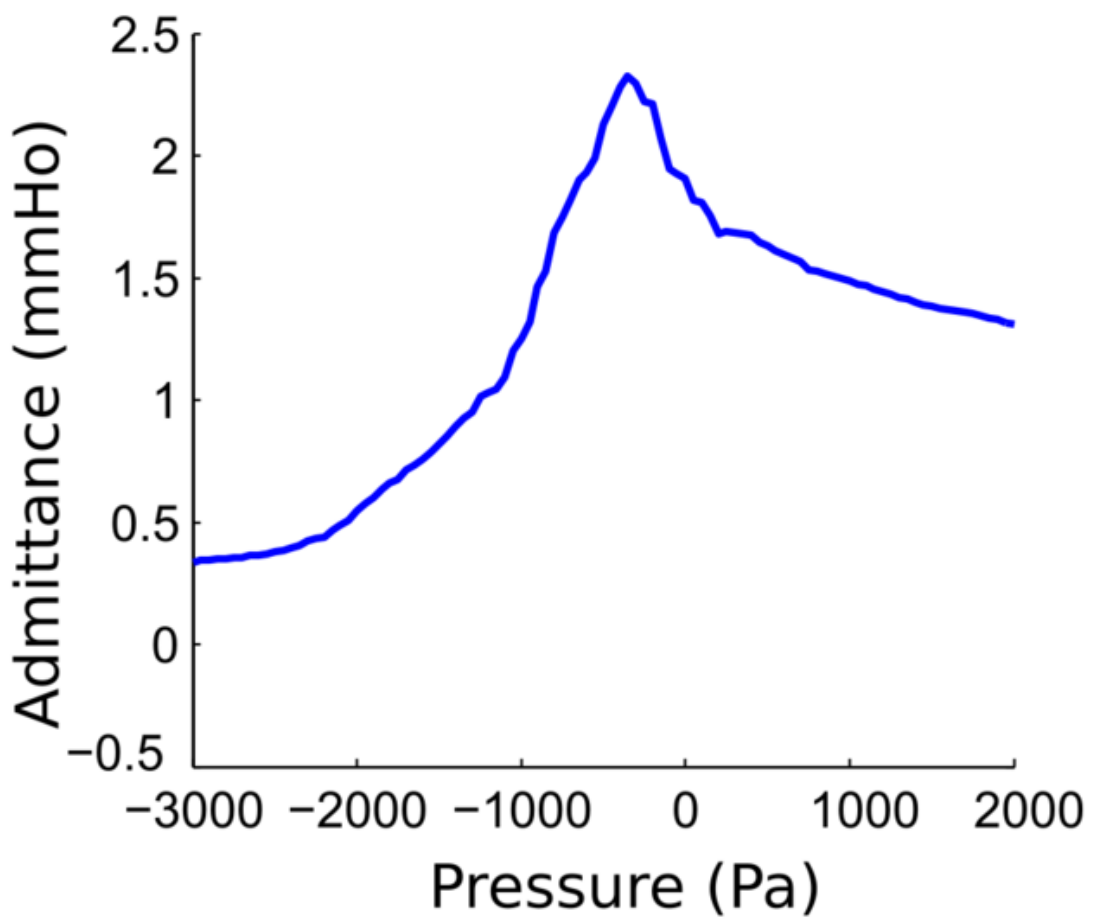


Figure 2

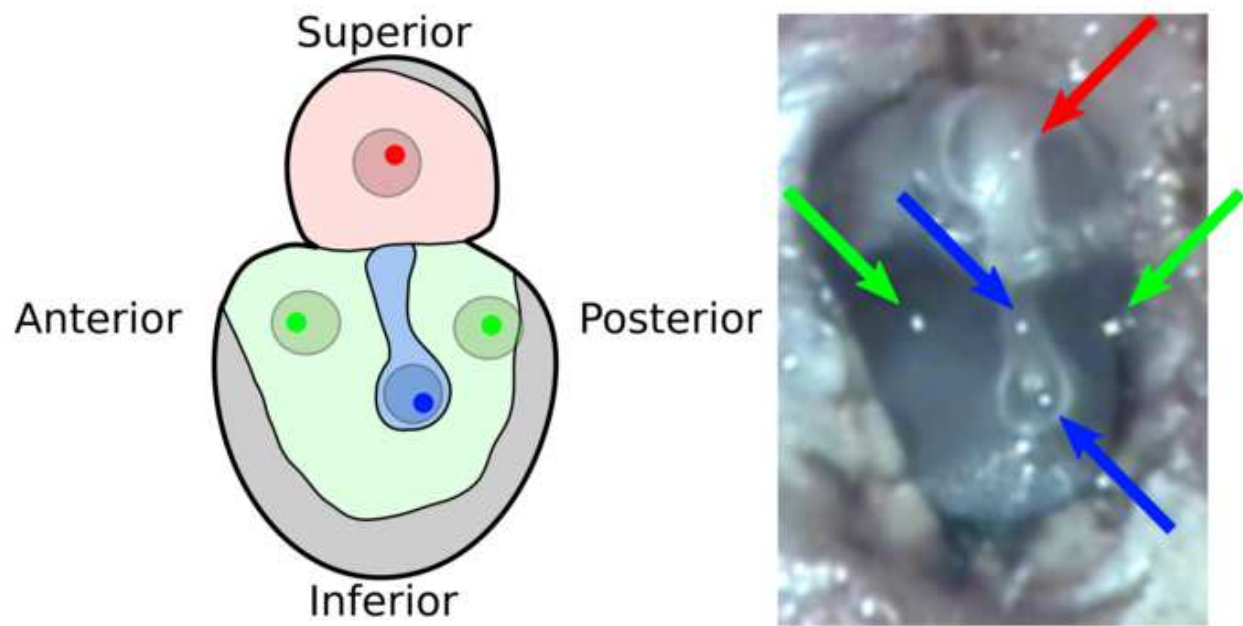


Figure 3

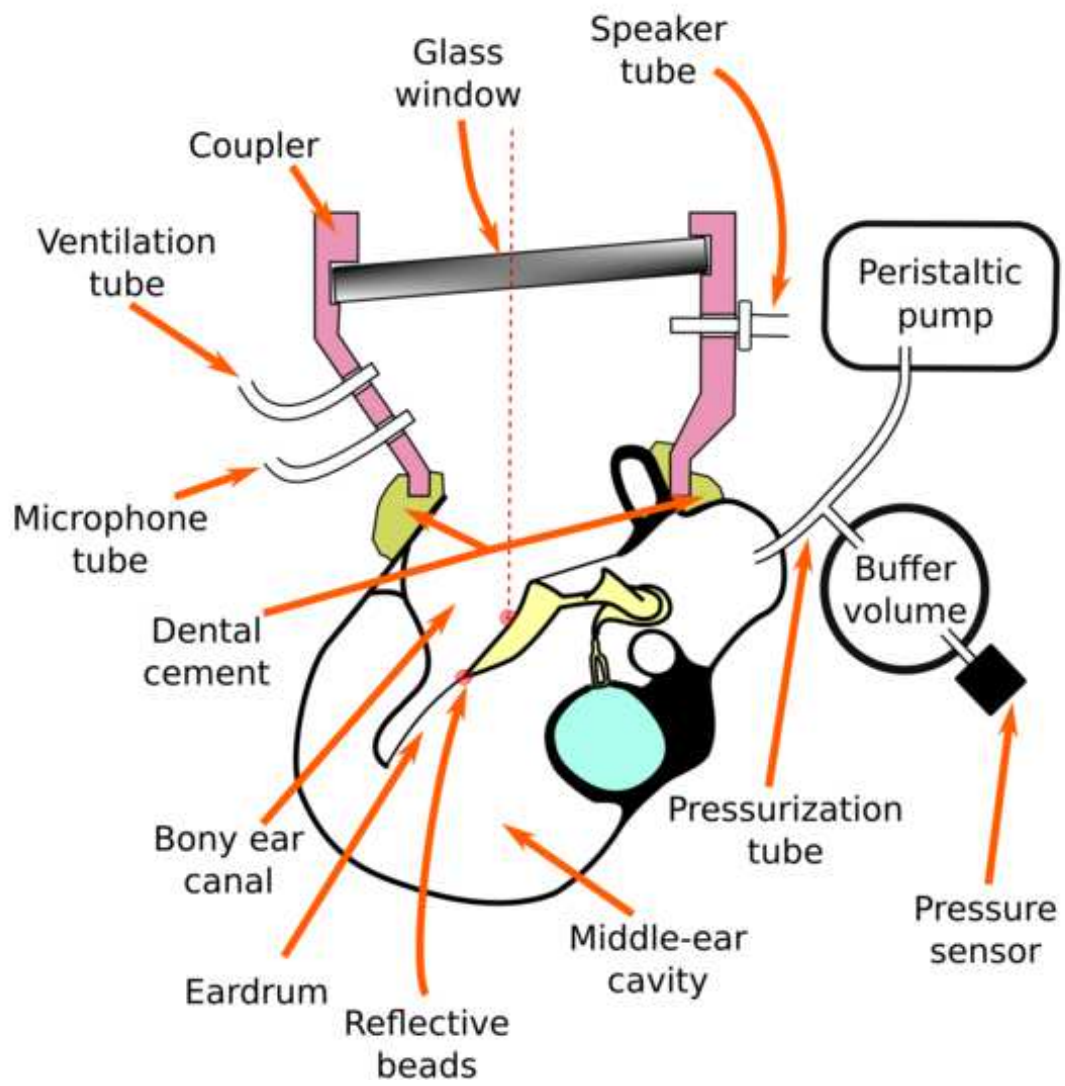


Figure 4

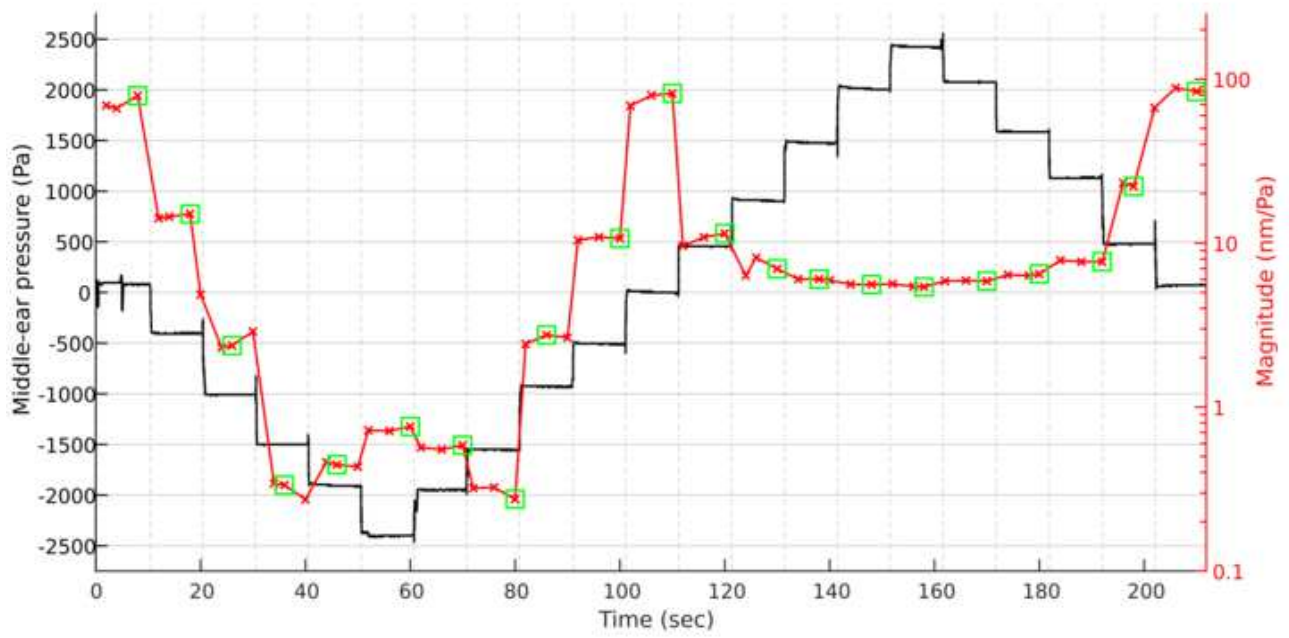


Figure 5

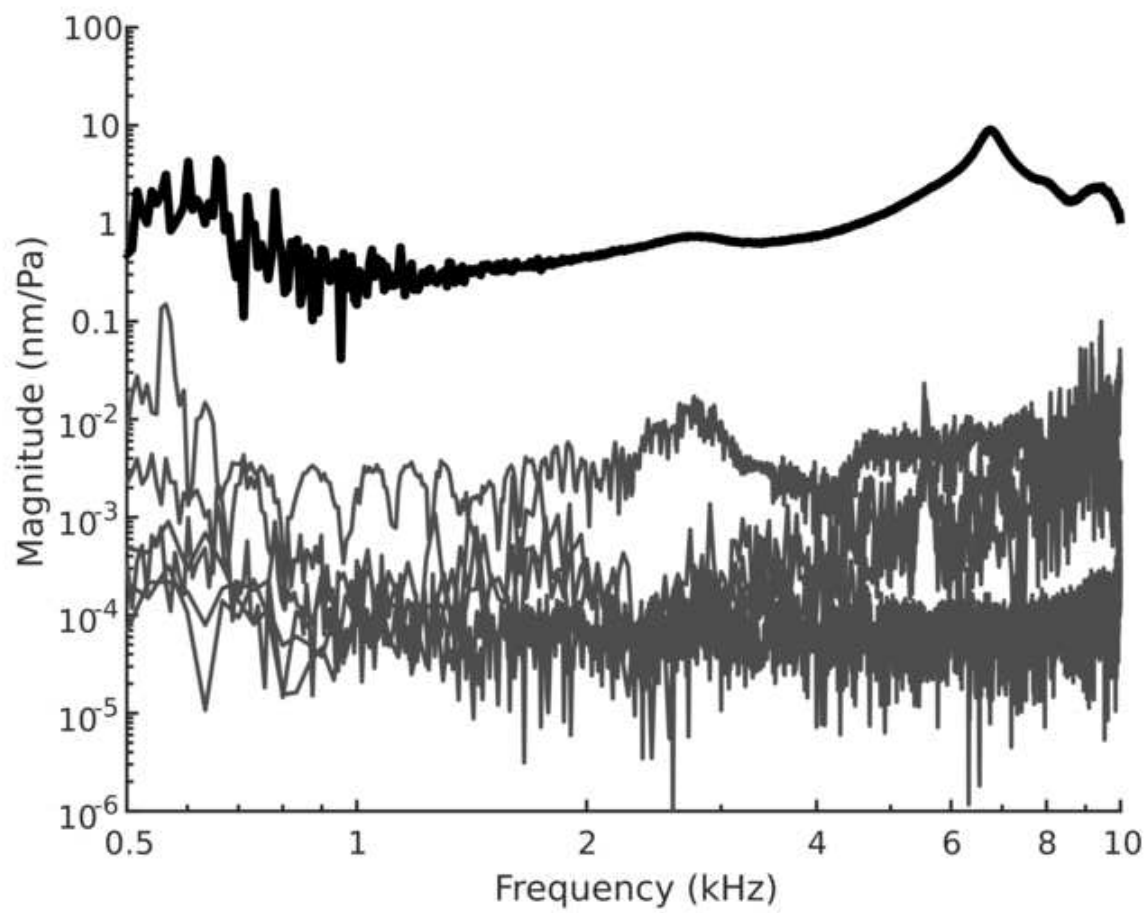


Figure 6

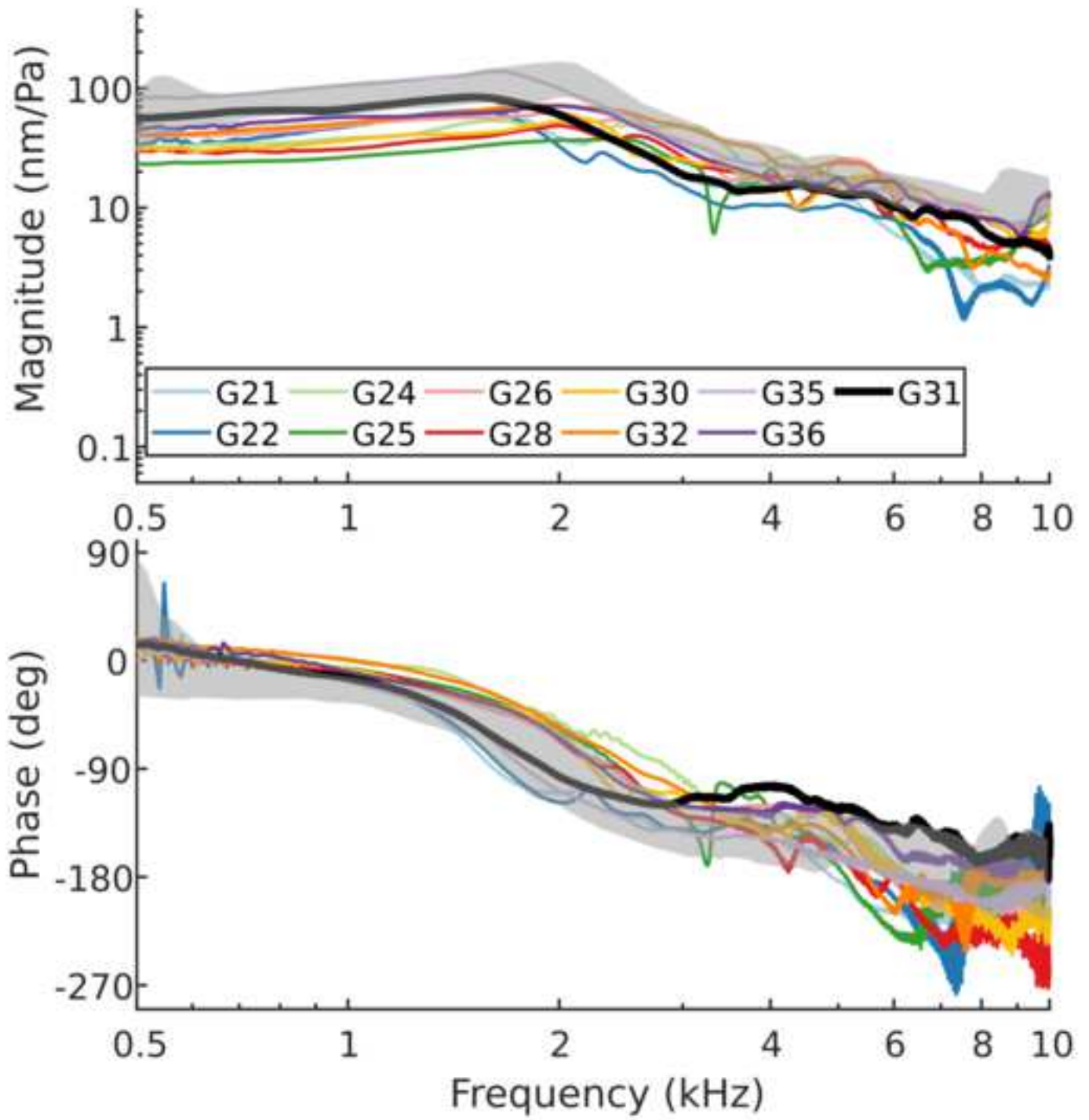


Figure 7

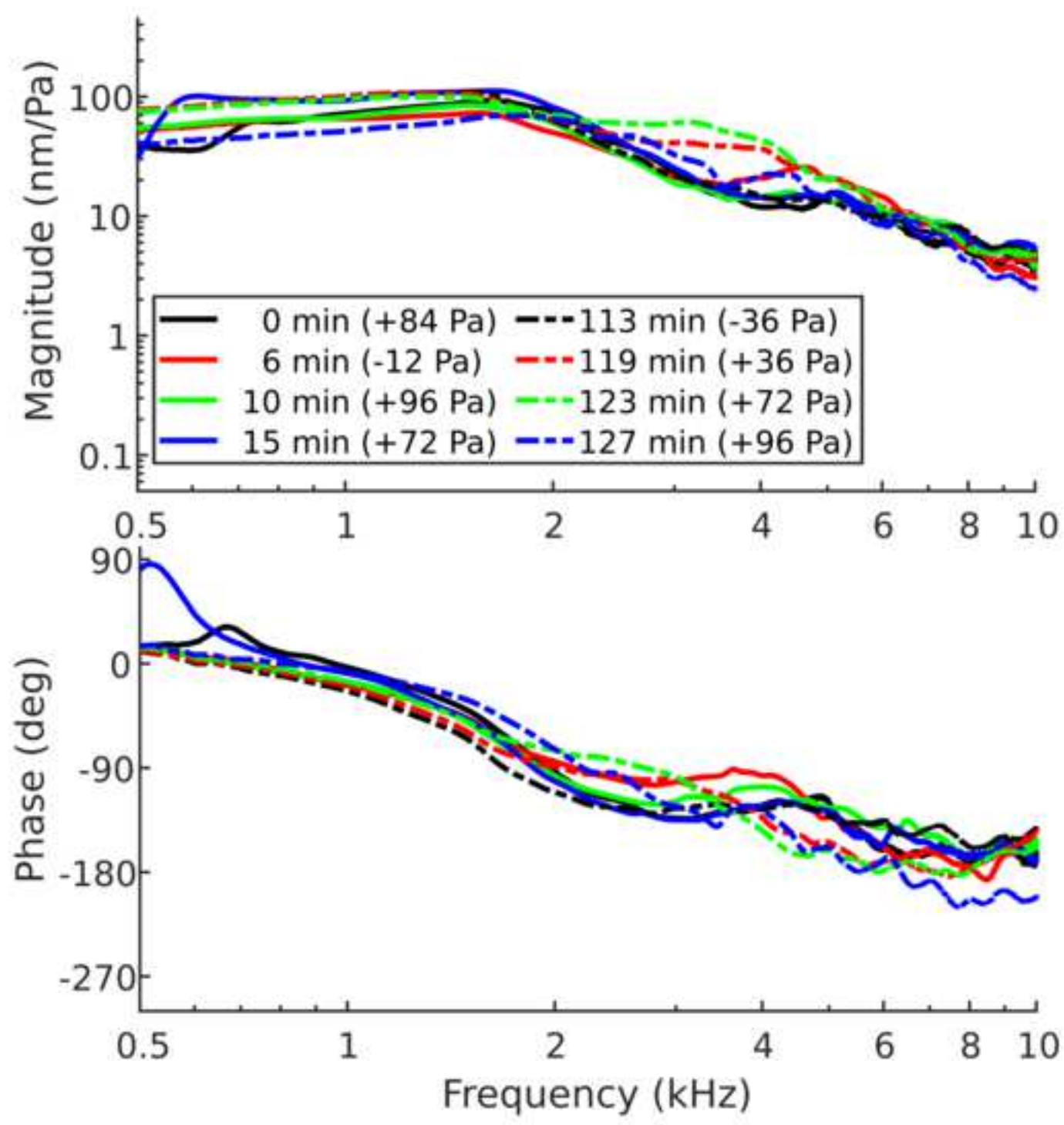


Figure 8

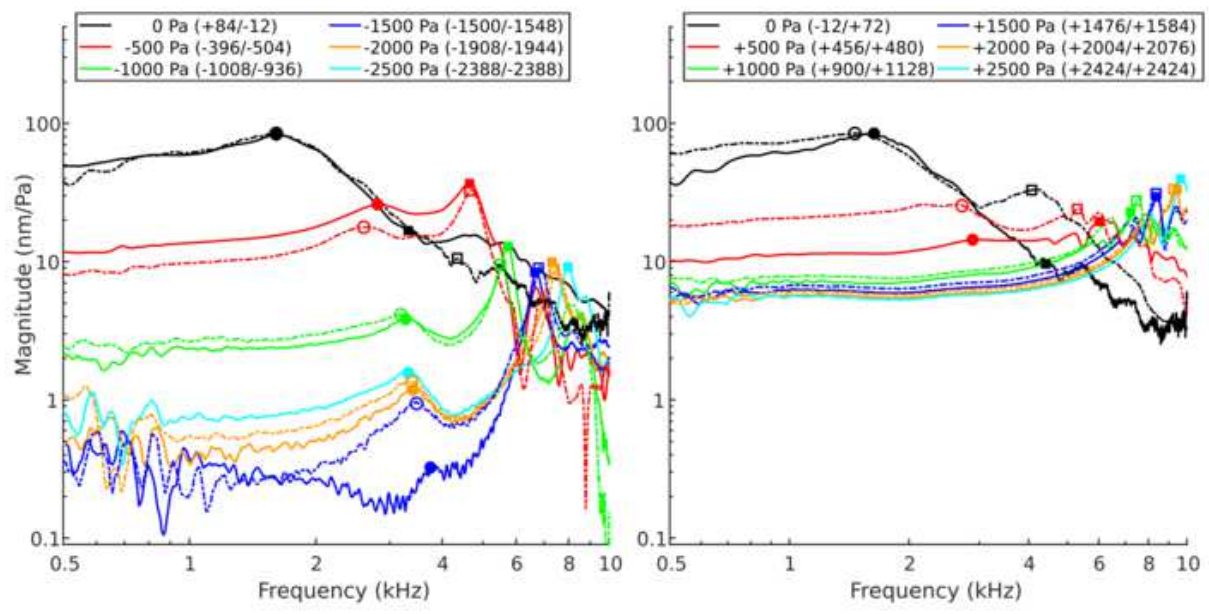


Figure 9

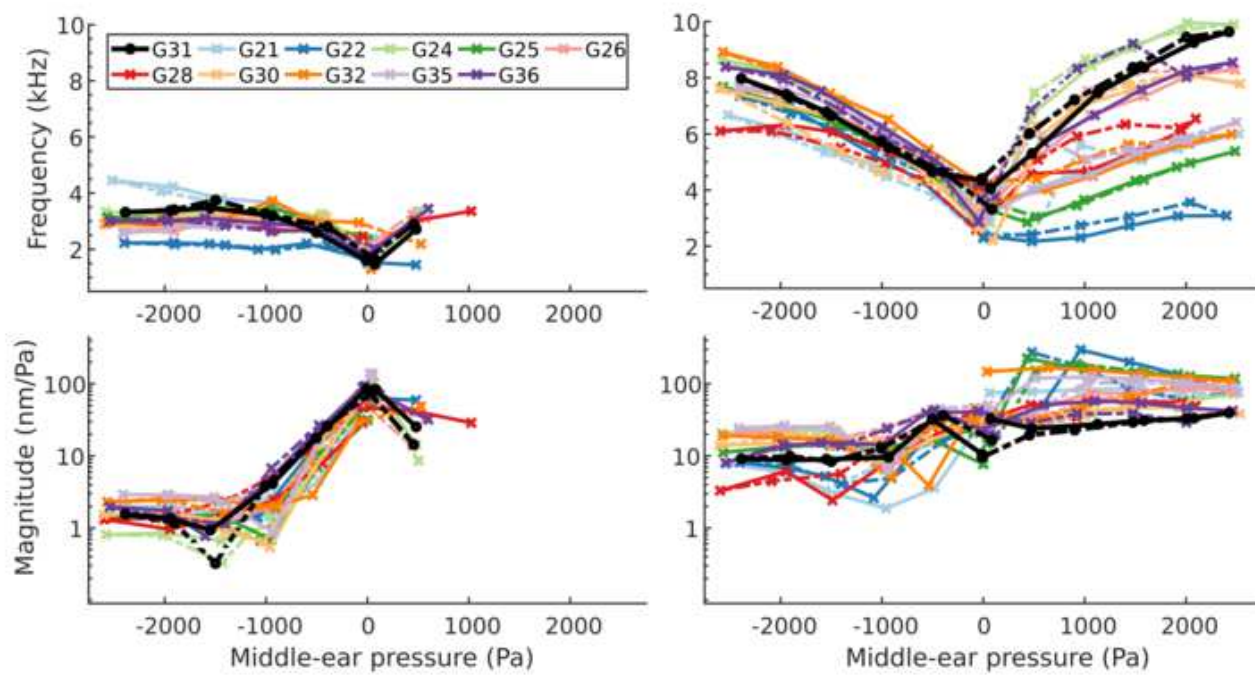
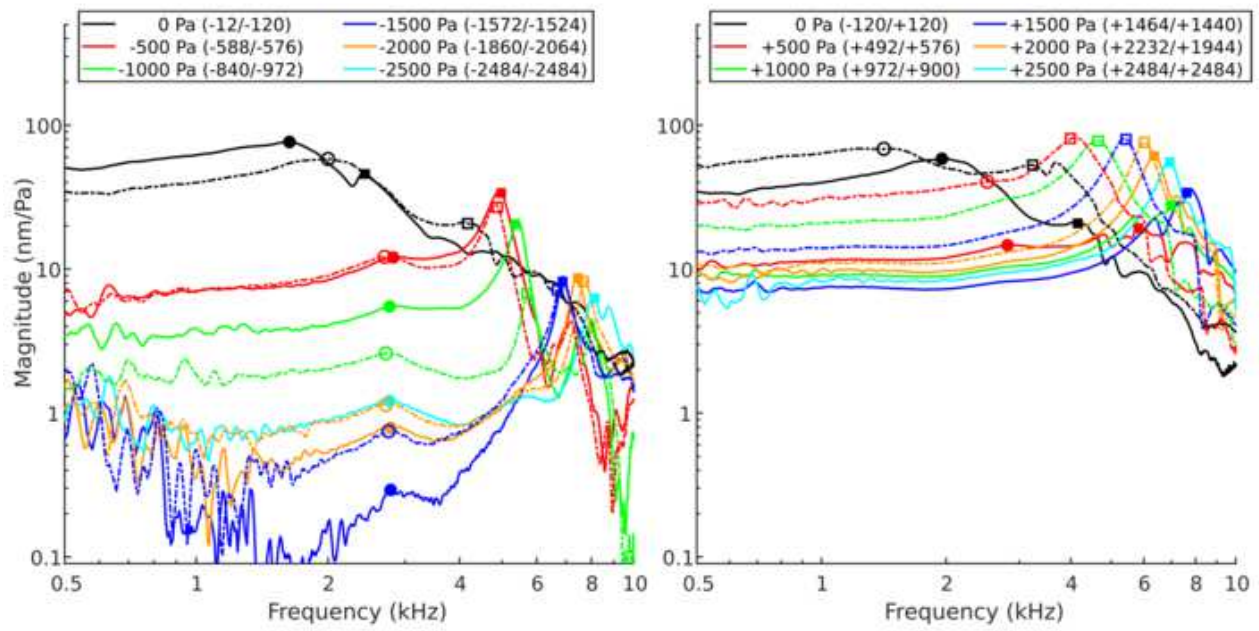


Figure 10



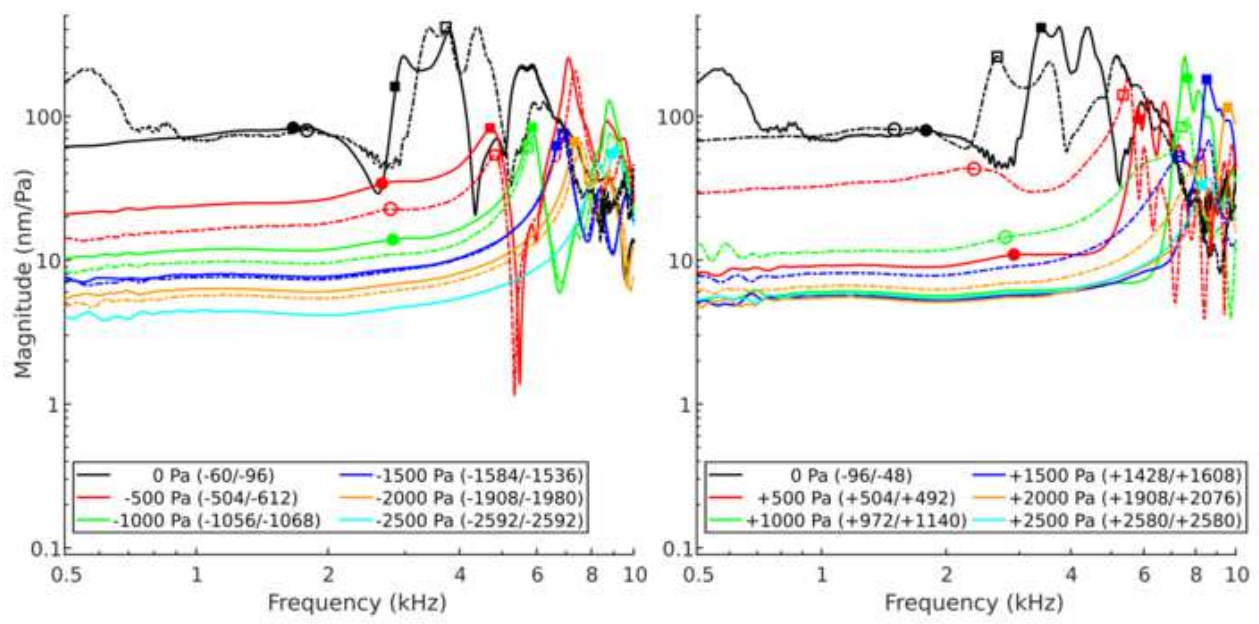


Figure 12

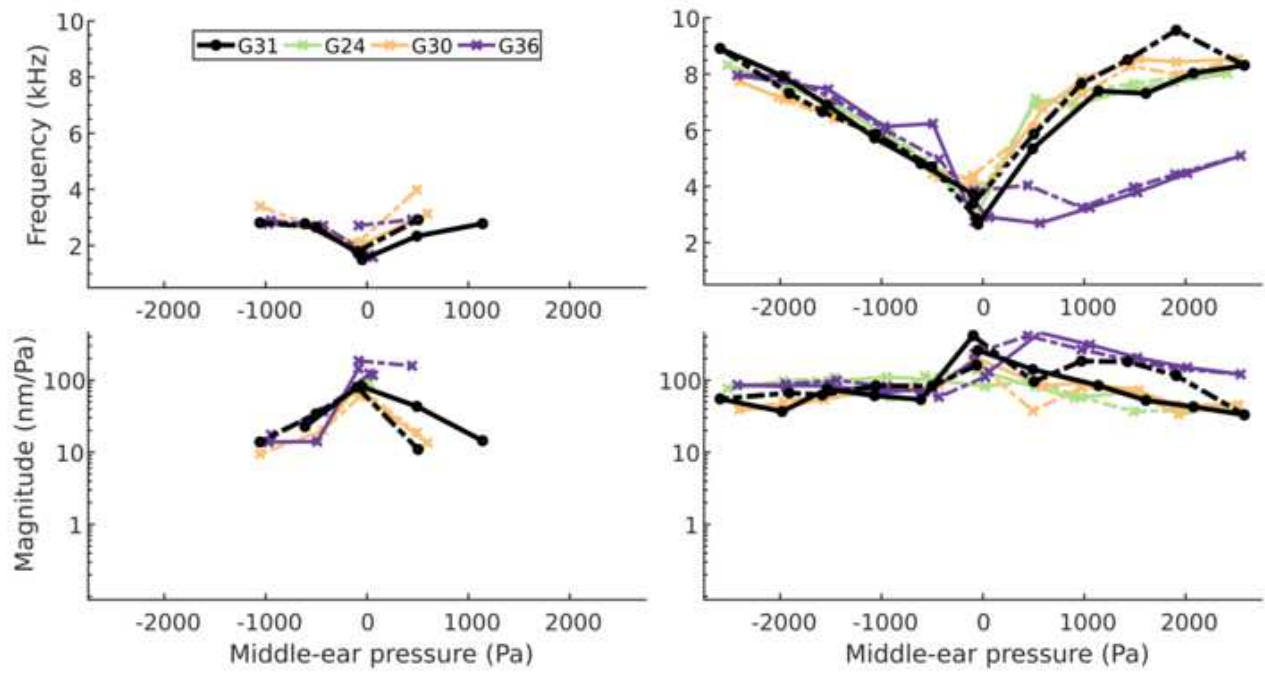


Figure 13

